**Research Article**

Hao Liu, Lars Jensen*, Ping Ma and Detlev Ristau

# ALD anti-reflection coatings at 1ω, 2ω, 3ω, and 4ω for high-power ns-laser application

https://doi.org/10.1515/aot-2017-0086
Received December 7, 2017; accepted January 16, 2018; previously published online March 21, 2018

**Abstract:** Atomic layer deposition (ALD) facilitates the deposition of coatings with precise thickness, high surface conformity, structural uniformity, and nodular-free structure, which are properties desired in high-power laser coatings. ALD was studied to produce uniform and stable $Al_2O_3$ and $HfO_2$ single layers and was employed to produce anti-reflection coatings for the harmonics (1ω, 2ω, 3ω, and 4ω) of the Nd:YAG laser. In order to qualify the ALD films for high-power laser applications, the band gap energy, absorption, and element content of single layers were characterized. The damage tests of anti-reflection coatings were carried out with a laser system operated at 1ω, 2ω, 3ω, and 4ω, respectively. The damage mechanism was discussed by analyzing the damage morphology and electric field intensity difference. ALD coatings exhibit stable growth rates, low absorption, and rather high laser-induced damage threshold (LIDT). The LIDT is limited by $HfO_2$ as the employed high-index material. These properties indicate the high versatility of ALD films for applications in high-power coatings.

**Keywords:** ALD $Al_2O_3$; ALD $HfO_2$; anti-reflection coating; LIDT.

## 1 Introduction

One of the challenges in using dielectric coatings in optical multilayer stacks is the realization of low absorption and high laser-induced damage thresholds (LIDTs). For example, the National Ignition Facility (NIF) is designed to achieve nearly 4 MJ of 1ω laser by 192 beam lines within several nanoseconds (ns) [1–4]. The optical components are presently the limiting factor for a further improvement in the output power of the system and are operated almost at their maximum power handling capability [5]. Furthermore, the coatings have to be prepared on large-aperture optics with a precise control of the optical thickness combined with a uniform thickness distribution.

Commonly, thin films applied in high-power optics are deposited by electron beam evaporation (EBE) [5]. EBE requires great technical efforts to meet strict tolerances in film thickness, uniformity, and power resistance, and *in situ* film growth monitoring is often necessary to ensure good reproducibility. Moreover, the intrinsic structural defects lead to optical losses [6, 7], and nodular defects contribute to the laser damage mechanisms [8]. Sol-gel porous $SiO_2$ films are mainly used as single-layer anti-reflection coatings with high LIDT [9, 10]. Ion beam sputtering (IBS) is widely used in low-loss/high-LIDT coatings with high packing density [11–13].

Atomic layer deposition (ALD) is considered to be a promising method for depositing optical thin films on account of its excellent thickness control, uniform growth over large areas, and small defect density. ALD is a chemisorptions-based deposition, in which the gaseous precursors are sequentially directed toward the substrate and chemisorbed by the local reactive ligands. The exposure of precursors is separated by purging pulses of inert gas. A typical ALD cycle consists of four steps: exposure of precursor, purging, exposure of reactant precursor, and followed by a second purging. Because of the limited amount of reactive ligands in each cycle, the growth of ALD is self-terminated in spite of the excessive precursors, enabling a precise control over film thickness without *in situ* monitoring. The gaseous precursors are extendible and have rather high diffusing rate, resulting in uniform coating with high packing density and few defects.

The development of ALD processes has been motivated mainly by microelectronics applications [14]. Though ALD has gained more attention in optical coatings in recent years [15–19], the properties of ALD films

***Corresponding author: Lars Jensen,** Laser Zentrum Hannover, Hollerithallee 8, 30419 Hannover, Germany, e-mail: l.jensen@lzh.de
**Hao Liu:** Laboratory of Nano and Quantum Engineering, Schneiderberg 39, 30167 Hannover, Germany
**Ping Ma:** Chengdu Fine Optical Engineering Research Center, Chengdu 610041, China
**Detlev Ristau:** Laser Zentrum Hannover, Hollerithallee 8, 30419 Hannover, Germany

regarding high-power laser are rarely reported [20–22]. Investigations in the optical properties and power handling capability of ALD coatings at prominent laser wavelengths gained importance during the last years. Moreover, the damage behavior of ALD coatings is expected to reveal further insights into ns-laser damage mechanism of coatings with minor structural defects.

Aluminum oxide ($Al_2O_3$) is the most studied and used material in ALD. The deposition is usually performed using TMA (trimethylaluminum) and water as precursors, which have excellent volatility and reactivity. This is almost an ideal self-terminating ALD process and often considered as a model system for ALD [14]. The large band gap of $Al_2O_3$ exemplifies it as a promising candidate for high-power coatings [23, 24]. Hafnium oxide ($HfO_2$) is one of the most widely accepted materials in high-power coating systems [5, 25]. ALD $HfO_2$ and $Al_2O_3$ can serve as a promising pair of high and low refractive index material for coating designs in high-power laser.

In this text, two-layer anti-reflection coatings working at 1064 nm, 532 nm, 355 nm, and 266 nm (1ω, 2ω, 3ω, and 4ω) have been prepared with ALD depositing $HfO_2$ and $Al_2O_3$. The properties of single layers as well as the anti-reflection coatings are analyzed. The LIDT, damage morphologies, and electrical field intensity (EFI) of the anti-reflection coatings are studied to investigate the damage mechanism.

# 2 Experiment

## 2.1 Atomic layer deposition

The ALD depositions were carried out at a substrate temperature of 200°C in an experimental vacuum chamber illustrated in Figure 1A. The precursors for $Al_2O_3$ were TMA (Trimethylaluminum, Dock Chemicals, Germany) and $H_2O$, and TEMAH (Tetraethylmethylaminohafnium, Pegasus, UK) and $H_2O$ were applied for $HfO_2$. Ar was selected as both purging gas and carrier gas for the precursors. High-precision flow controllers were employed to adjust the Ar flow rate, flow time, and flow path, either through precursor bubblers or directly into the chamber. The chamber pressure was maintained at 1 mbar by keeping the gas flow constant. The four steps in an ALD cycle (exposure, purging, exposure and purging) are illustrated in Figure 1B.

The chemisorption mechanisms of ALD $Al_2O_3$ and $HfO_2$ are illustrated in the reaction equation (1). A pulse of precursor vapor is dosed onto the substrate in an exposure step, and subsequently, a self-terminating chemisorbed monolayer with reactive ligands is formed. In the following purging step, the excessive precursor and byproducts are removed from the chamber by an Ar flow in order to avoid chemical vapor deposition, which might lead to uncontrolled film growth and non-uniformity.

$$
\begin{aligned}
&-\mathrm{Al}-\mathrm{OH} + \mathrm{Al(CH_3)_3} \rightarrow -\mathrm{Al}-\mathrm{O}-\mathrm{Al}-\mathrm{CH_3} + \mathrm{CH_4}\\
&-\mathrm{Al}-\mathrm{O}-\mathrm{Al}-\mathrm{CH_3} + \mathrm{H_2O} \rightarrow -\mathrm{Al}-\mathrm{O}-\mathrm{Al}-\mathrm{OH} + \mathrm{CH_4}\\
&-\mathrm{Hf}-\mathrm{OH} + \mathrm{Hf[N(CH_3CH_2CH_3)]_4} \rightarrow -\mathrm{Hf}-\mathrm{O}-\mathrm{Hf}-\mathrm{NCH_3CH_2CH_3}\\
&\qquad\qquad + \mathrm{HNCH_3CH_2CH_3}\\
&-\mathrm{Hf}-\mathrm{O}-\mathrm{Hf}-\mathrm{NCH_3CH_2CH_3} + \mathrm{H_2O} \rightarrow -\mathrm{Hf}-\mathrm{O}-\mathrm{Hf}-\mathrm{OH} + \mathrm{HNCH_3CH_2CH_3}
\end{aligned}
\tag{1}
$$

Single layers have been prepared for studying the optical constants of ALD $HfO_2$ and $Al_2O_3$. 1ω, 2ω, 3ω and 4ω anti-reflection coatings were designed by optimizing the basic V-type two layer AR-coatings: Substrate/$HfO_2$/$Al_2O_3$/Air. The optical properties of anti-reflection coatings as well as single layers were characterized.

## 2.2 Characterization

The transmittance and reflectance spectra were recorded in a wavelength range of 200–2000 nm using a PerkinElmer LAMBDA 950 spectrophotometer (PerkinElmer, MA, USA). The measurement accuracy of the spectrophotometer is about ±0.2%. From the spectra of single layers, the refractive indices $n$ and extinction coefficients $k$ of ALD $HfO_2$ as well as $Al_2O_3$ were determined. The film thicknesses were fitted from the spectra and compared with the initial coating designs.

The elemental composition was assessed by energy-dispersive X-ray spectroscopy (EDX, FEI, OR, USA), in which the energy

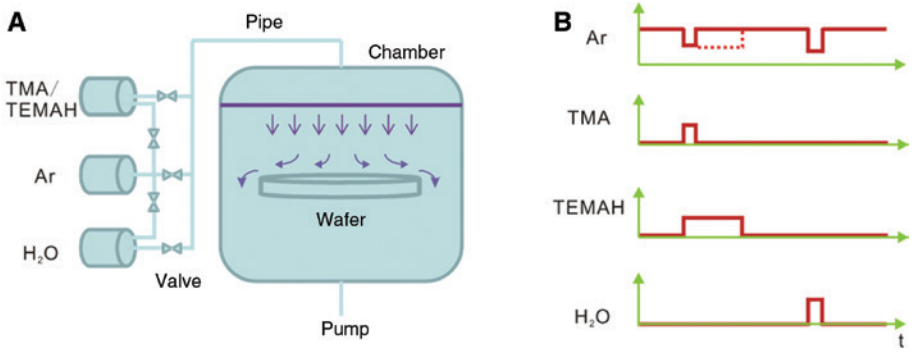


**Figure 1:** The valves control the flow of Ar, either through precursors or directly into the chamber. The pressure is kept still in the chamber. (A) Schematic of ALD system; (B) schematic of gas flow during one ALD cycle.

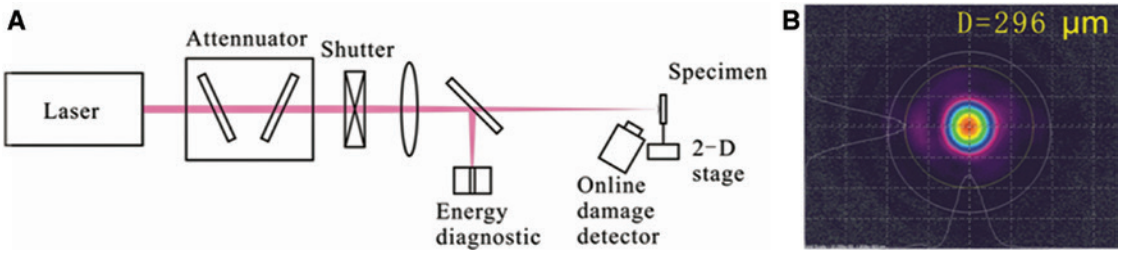


**Figure 2:** The beams with different fluence irradiate the specimen, and the online detector judges if the damage occurs. (A) LIDT test bench; (B) beam spot of 1ω laser.

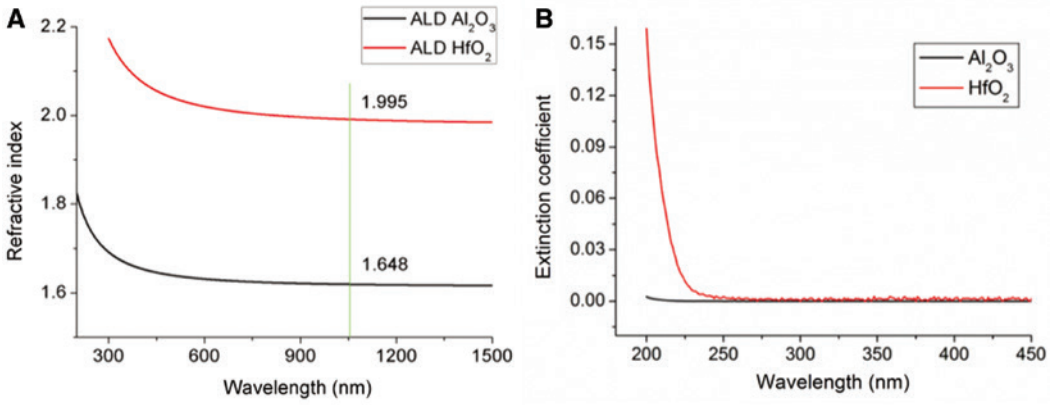


**Figure 3:** Dispersion comparison of ALD $HfO_2$ and $Al_2O_3$. The refractive index difference is about 0.35. The absorption edge of $HfO_2$ is at about 230 nm. (A) Refractive index; (B) extinction coefficient.

difference between two shells of an atom is measured to determine the element. As a consequence of the single shell configuration, the first two elements in the periodic table, H and He, cannot be detected by this method. Carbon contents may be present in the form of $-CH_3$ in the $Al_2O_3$ films and as $-NCH_3CH_2CH_3$ in the $HfO_2$ films, respectively. Excessive oxygen is expected to be bound in –OH complexes.

Band gap energies were determined by extrapolating the linear region of the Tauc plot to the abscissa. The Tauc plot is based on the quantity $h\upsilon$ (the energy of photon) on the abscissa and the quantity $(\alpha h\upsilon)^{1/2}$ on the ordinate, in which $\alpha$ is the absorption coefficient in the deep UV range [26].

Weak absorption was measured using laser calorimetry according to ISO 11551 [27, 28]. The 1ω, 2ω, 3ω anti-reflection coatings were characterized by the 1ω, 2ω, and 3ω lasers, respectively. The absolute error was about 13%.

S-on-1 LIDT values were measured with a test bench setup according to ISO 21254 [29] (Figure 2A). The pulse width was adjusted to 10 ns, the repetition frequency was fixed to 100 Hz, and the beam was focused to an effective diameter of about 300 μm (Figure 2B, 1ω laser spot). For damage detection, a scattering measurement system was employed that also triggers a stop of the laser irradiation of the test site as soon as damage is detected. The overall 154 sites were

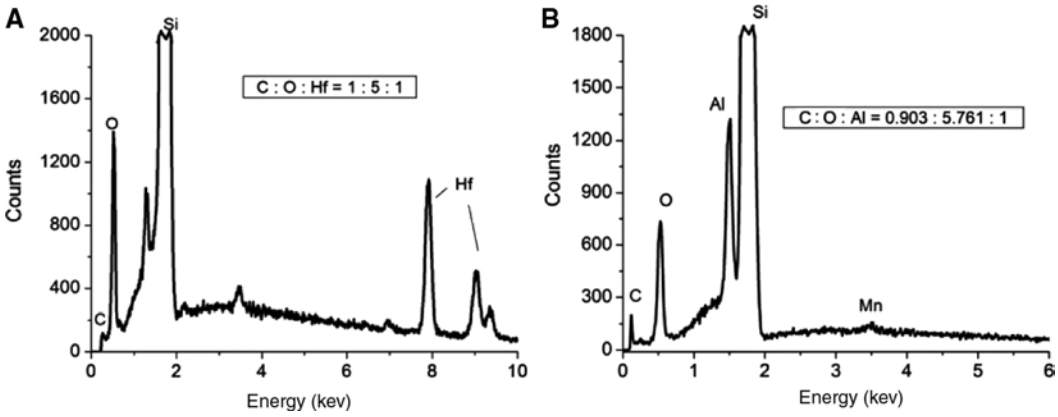


**Figure 4:** The substrate, film material and precursor residuals are detected. EDX characterization of (A) ALD $HfO_2$ and (B) $Al_2O_3$.

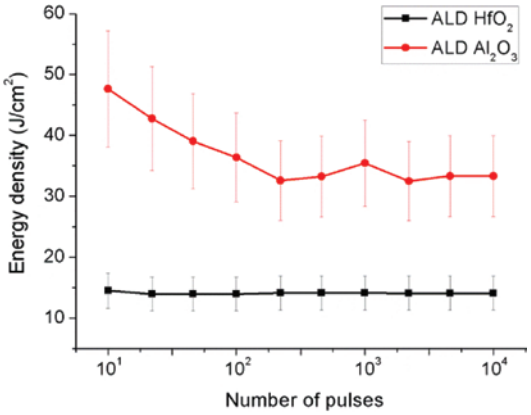


**Figure 5:** Damage characteristic of ALD $HfO_2$ and $Al_2O_3$ single layers.

tested on each sample. Together with each site, the beam energy and detected scattering of each pulse were recorded. Damage was confirmed if the detected scattering exceeded a threshold value and reconfirmed by Nomarski microscope inspection (Leica Microsystems, Wetzlar, Germany) after the test.

The damage probability was statistically calculated and plotted versus the energy density for each sample. The LIDT was determined by extrapolating the fit of damage probability to the abscissa. The absolute error is about 20% and mainly governed by the fluence measurement. Damage morphologies were characterized with either differential interference contrast (DIC) microscopy or confocal laser scanning microscopy (LSM).

# 3 Results and discussion

## 3.1 Single layers

The dispersion curves of ALD $HfO_2$ and $Al_2O_3$ are displayed in Figure 3 for comparison. The difference of the refractive index is about 0.35 at 1064 nm, a sufficient value for optical coating designs. The absorption edge of ALD $HfO_2$ ranges to wavelengths around 230 nm, while $Al_2O_3$ reaches values well below 200 nm. ALD $HfO_2$ is, therefore, a suitable material for optical components working at 1ω–4ω; however, it exhibits severe absorption at 5ω or shorter wavelengths.

The spectra in the deep UV range enable the determination of band gap energy $E_{gap}$ via the Tauc plot method. The $E_{gap}$ value of ALD $HfO_2$ amounts to 5.5 eV and of $Al_2O_3$ to 6.5 eV, respectively. These data are in agreement with the IBS $HfO_2$ and $Al_2O_3$ films [30].

The measured EDX curves are shown in Figure 4. Nitrogen is not detected and expected to contribute only a small content. Precursor ligands $-CH_3$ and $-NCH_3CH_2CH_3$

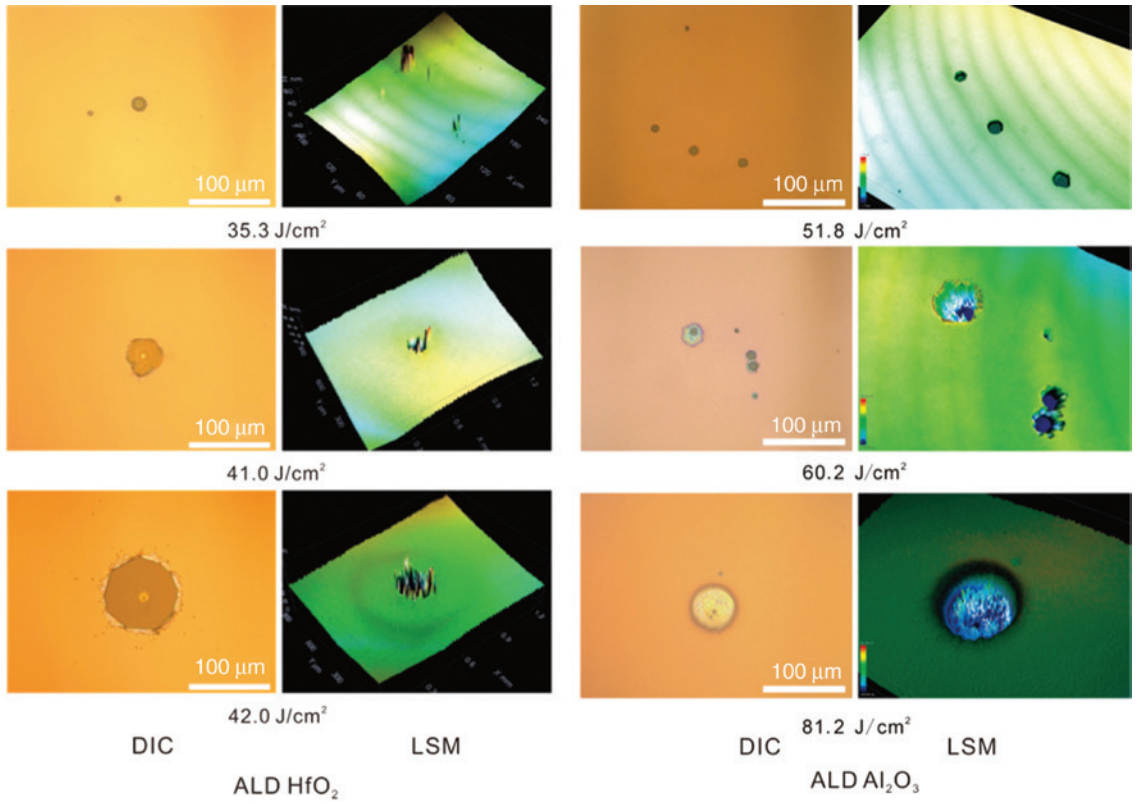


**Figure 6:** Damage morphologies of ALD $HfO_2$ and $Al_2O_3$ single layers. The damage morphologies at low fluences are pits, while at higher fluences are burning scalds.

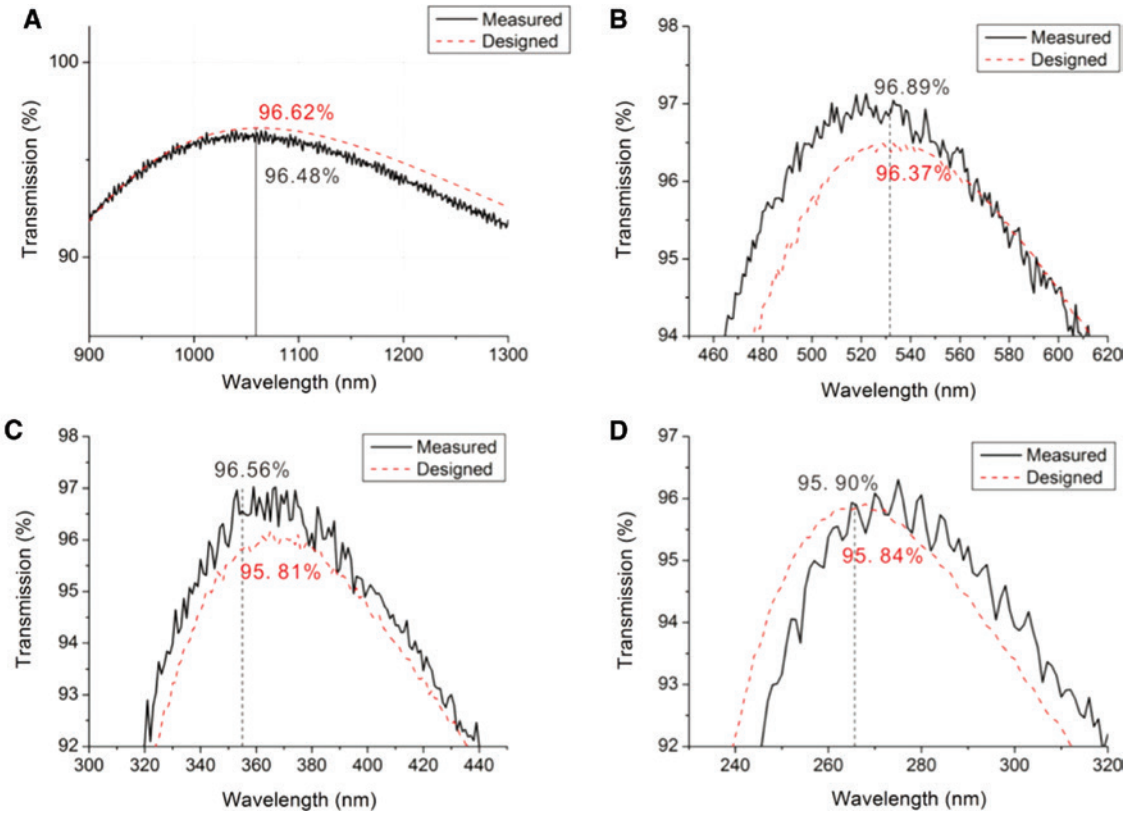


**Figure 7:** Comparison of designed and measured spectra of anti-reflection coatings. The measured spectra match the designs well, with slight deviations. (A) 1ω; (B) 2ω; (C) 3ω; (D) 4ω.

are detected. These precursor ligands have two possible origins: some of the precursor or byproduct molecules are physisorbed on the substrate and not converted by chemisorption; some of the reactive ligands are shielded by the neighboring molecules.

Laser calorimetric tests at a wavelength of 1064 nm show that both films have absorption values smaller than 3 ppm, which is a small value indicating the promising application in high-power components. Basically, the used fused silica substrates contribute this level of absorption. Therefore, the film absorption can be estimated to range between 1 and 2 ppm.

The characteristic damage curves of ALD $HfO_2$ and $Al_2O_3$ at a wavelength of 1064 nm are shown in Figure 5. ALD $Al_2O_3$ indicates a distinctively higher LIDT than $HfO_2$. For irradiation with 10 pulses, the LIDT of $Al_2O_3$ is 46 J/cm² compared to 14 J/cm² of $HfO_2$. The LIDT decreases, in general, as the pulse number increases, due to fatigue effect.

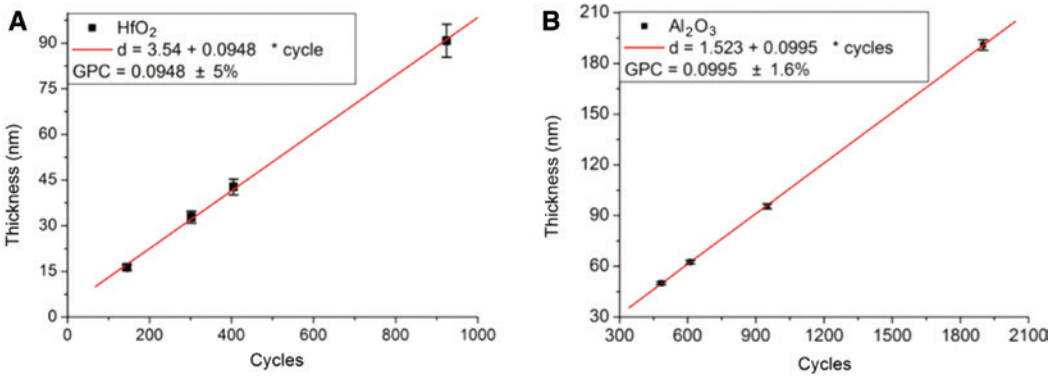


**Figure 8:** Growth rate of single layers. Film thickness grows linearly with number of cycles. (A) ALD $HfO_2$; (B) ALD $Al_2O_3$.

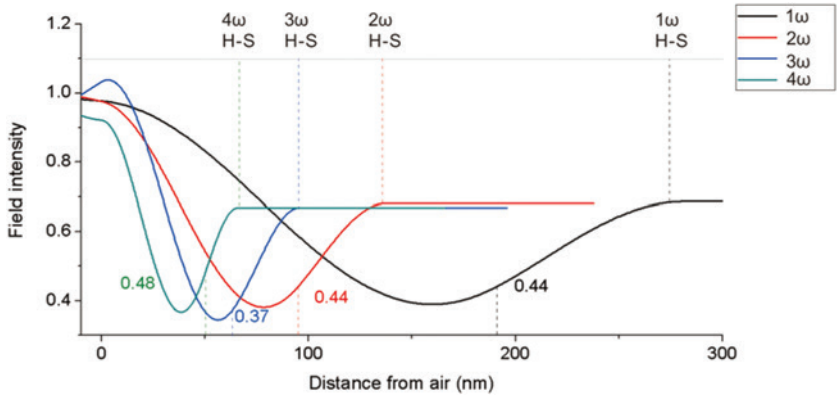


**Figure 9:** Electrical field intensity distribution in the anti-reflection coatings.
The curves start from the air-$Al_2O_3$ surfaces. The $Al_2O_3$-$HfO_2$ and $HfO_2$-substrate interfaces are marked (calculated using Spektrum, LZH, Hannover, Germany).

Our previous study showed that ALD single layers have generally slightly higher LIDT than IBS layers at a wavelength 1064 nm. In comparison, the fused silica substrate has an LIDT above 70 J/cm$^2$ [24].

The damage morphologies caused by single pulses are shown in Figure 6. The LSM characterization provides three-dimensional (3D) images of the same sites inspected with DIC images. For low fluence irradiation, the morphologies are characterized by discrete pits with average diameters in the range of 10 μm. For higher fluences, larger size scalds are formed. The morphologies indicate that the damage is initiated by defects, on both ALD $HfO_2$ and $Al_2O_3$ film.

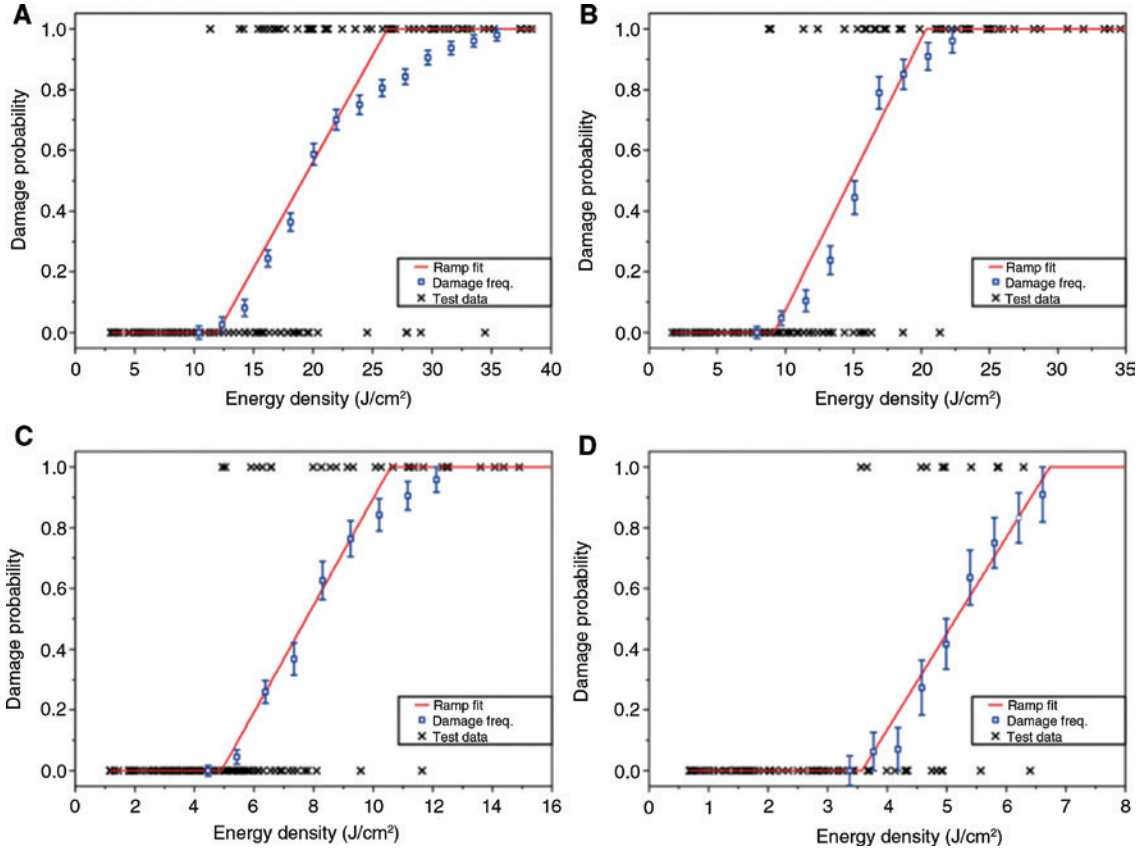


**Figure 10:** Damage probabilities of the anti-reflection coatings irradiated by 10 pulses of different wavelength lasers. (A) 1ω; (B) 2ω; (C) 3ω; (D) 4ω.

## 3.2 Anti-reflection coatings

The transmittance of the 1ω, 2ω, 3ω, and 4ω anti-reflection coatings are shown in Figure 7. The measured spectra match the designed curves very well, indicating a precise control of the ALD process over film thickness without *in situ* monitoring. The measured 1ω, 2ω, and 3ω transmission including back-surface reflection approximates the ideal value of 96.5% for fused silica substrates with a single-side anti-reflection coating. The transmission of the anti-reflection coating for 4ω is slightly lower, partly due to the design error finding a local optimization, and partly due to the larger refractive index of the substrate at shorter wavelengths. The spectra indicate good applicability of the ALD coatings for the NUV to the NIR wavelength range.

Recalculation of the measurement shows about 5% error in $HfO_2$ thickness and about 1% error in $Al_2O_3$ thickness. From the analysis, it is expected that this error originates from the incomplete purging of $H_2O$ in the ALD process. TEMAH has larger condensing rate than TMA, therefore, influencing the thickness of $HfO_2$ more than $Al_2O_3$. The film thicknesses are plotted with depositing cycles, showing the GPC (growth per cycle) of $HfO_2$ 0.0948 nm and $Al_2O_3$ 0.0995 nm (Figure 8).

The electrical field intensity EFI distributions in the coatings are illustrated in Figure 9. The central wavelengths of the anti-reflection coatings are selected for the calculation. The four EFI distributions have a similar shape from the air-film surface to film-substrate surface. The $Al_2O_3$-$HfO_2$ surface of each coating is marked in the figure. The EFI in the $HfO_2$ layers have a rather close value among the coatings. The EFI should not cause distinct differences in the LIDT among the 1ω, 2ω, 3ω, and 4ω anti-reflection coatings.

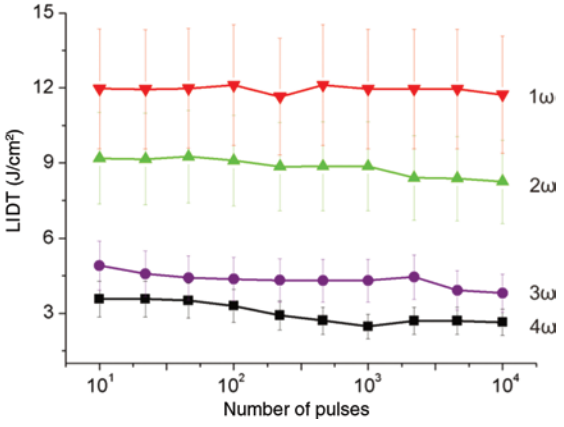


**Figure 11:** Characteristic damage of anti-reflection coatings.

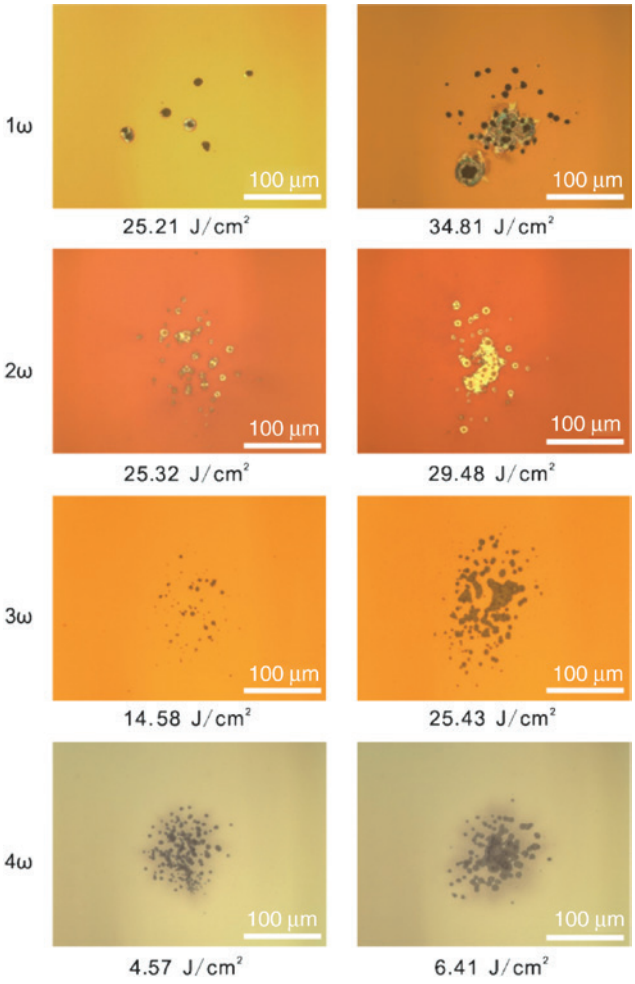


**Figure 12:** Damage morphologies of anti-reflection coatings. The morphologes at low fluences are pits while at high fluences are scalds.

The 1ω anti-reflection coating has an absorption of about 1 ppm at a wavelength of 1ω. The 2ω and 3ω anti-reflection coatings have absorptions of 9.3 ppm and 597.1 ppm at wavelengths of 2ω and 3ω, respectively. Laser calorimetry measures the average absorption on the sample within the irradiation spot. The ALD coatings have rather small absorption indicating a promising application in low-loss and high-power coatings.

The damage probability plots of the anti-reflection coatings irradiated with 10 pulses are shown in Figure 10. The LIDT is determined close to the highest fluence causing no damage, which is generally defined as the 0% LIDT [29]. The LIDT of 1ω, 2ω, 3ω, and 4ω anti-reflection coatings are about 12, 9, 4.5, and 3.4 J/cm² at wavelengths of 1ω, 2ω, 3ω, and 4ω, respectively. The LIDT values are probably limited by the $HfO_2$ film. Some testing sites survive rather high fluence, indicating the potential of LIDT improvement if the defects are controlled. The

**Table 1:** Property summary of ALD coatings.

| | Fused silica at 1ω | ~130 nm $HfO_2$ at 1ω | ~320 nm $Al_2O_3$ at 1ω | 1ω AR at 1ω | 2ω AR at 2ω | 3ω AR at 3ω | 4ω AR at 4ω |
|---|---|---|---|---|---|---|---|
| Transmission (%) | – | – | – | 96.5 | 96.9 | 96.6 | 95.9 |
| $E_{gap}$ (eV) | 7.5 | 5.5 | 6.5 | – | – | – | – |
| Absorption (ppm) | <1 | <3 | <3 | ~1 | 9.3 | 597.1 | – |
| LIDT, 10 pulses (J/cm²) | 72 | >40 | 14.0 | 12.0 | 9.2 | 4.9 | 3.6 |

characteristic damage curves are compared in Figure 11. Irradiation with a shorter wavelength induces a distinctively lower LIDT. The LIDT values decrease slightly as the pulse number increases as a result of the fatigue effect.

The damage morphologies of the anti-reflection coatings are shown in Figure 12. The 1ω, 2ω, and 3ω morphologies are taken after 1 pulse irradiation, while the two images of 4ω morphologies were recorded for a site irradiated by four pulses and 23 pulses, respectively. The morphologies indicate that defects induced damage in all samples. Low fluences induce small pits, while higher fluences burn scalds around the pits. The defects initiating damage appear with larger density for shorter wavelengths.

### 3.3 Discussion

The properties of the investigated coatings are summarized in Table 1. ALD $HfO_2$ and $Al_2O_3$ have large band gap energies $E_{gap}$, low absorption, and a promising LIDT. Though the LIDTs of anti-reflection coatings are not the highest among the different coating techniques [31], the decent properties of ALD coatings, such as self-terminating and high density, can contribute together with their distinct characteristics to optical and high-power laser applications. With these films, it was the goal to collect first data on the potential of the ALD films for laser applications. The next step is to optimize the plant and the applied process to achieve low defect concentrations.

The damage of both the ALD single layers and anti-reflection coatings are induced by defects. The damage morphologies shown in Figure 12 show a rather high defect density especially for the UV test samples. This is consistent with the general opinion of damage mechanisms often observed in the ns-pulse regime [32]. This text provides findings on how these mechanisms also apply for ALD films. However, it is planned for future work to drive the ALD process with its potential for a low defect density film growth to a status where the defect-induced damage might not be as dominant anymore.

## 4 Conclusion

Because of its precise thickness control and nodular-free film structure, the ALD coatings have promising applications in high-power laser systems and corresponding laser damage investigations. ALD $HfO_2$ and $Al_2O_3$ have been prepared and characterized. Both ALD $HfO_2$ and $Al_2O_3$ have large band gap, low absorption, and relatively high LIDT at 1ω wavelength.

The anti-reflection coatings for the harmonics of the Nd:YAG laser 1ω, 2ω, 3ω, and 4ω have been deposited without *in situ* monitoring. The measured spectra proved the precise control over thickness on the basis of cycle counting. The respective LIDT tests at 1ω, 2ω, 3ω, and 4ω revealed promising results for an application of ALD coatings in high-power optics from the NUV to the NIR spectral range.

## References

[1] D. H. Crandall, C. J. Keane, K. Bieg, L. V. Powers and M. M. Sluyter, Proc. SPIE 3047, 2–13 (1997).
[2] M. Bowers, J. Wisoff, M. Herrmann, T. Anklam, J. Dawson, et al., Proc. SPIE 10084, 1008403 (2017).
[3] J. A. Horvath, Proc. SPIE 3047, 148–157 (1997).
[4] V. Denis, V. Beau, L. L. Deroff, L. Lacampagne, T. Chies, et al., Proc. SPIE 10084, 1008401 (2017).
[5] C. J. Stolz, C. L. Weinzapfel, A. L. Rigatti, J. B. Oliver, J. Taniguchi, et al., Proc. SPIE 5193, 50–58 (2004).
[6] C. J. Stolz, J. R. Taylor, W. K. Eickelberg and J. D. Lindh, Appl. Opt. 32(28), 5666–5672 (1993).
[7] I. Petrov, P. B. Barna, L. Hultman and J. E. Greene, J. Vac. Sci. Technol. A 21(5), S117–S126 (2003).
[8] C. J. Stolz, L. M. Sheehan, S. M. Maricle, S. Schwartz, M. R. Kozlowski, et al., Proc. SPIE 3264, 105–112 (1998).
[9] P. A. Sermon, M. S. W. Vong, N. J. Bazin, R. Badheka and D. M. Spriggs, Proc. SPIE 2633, 464–474 (1995).
[10] M. R. Kozlowski and I. M. Thomas, Proc. SPIE 2262, 54–59 (1994).
[11] F. Beauville, D. Buskulic, R. Flaminio, F. Marion, A. Masserot, et al., Proc. SPIE 5250, 483–492 (2004).
[12] M. Sigwarth, J. Baumgartner, A. Bell, G. Cagnoli, A. Fischer, et al., Proc. SPIE 9908, 99084F (2016).

[13] R. A. Negres, C. J. Stolz, M. D. Thomas and M. Caputo, Proc. SPIE 10447, 104470x (2017).
[14] V. Miikkulainen, M. Leskelä, M. Ritala and R. L. Puurunen, J. Appl. Phys. 113, 021301 (2013).
[15] A. Szeghalmi, M. Helgert, R. Brunner, F. Heyroth, U. Gösele, et al., Appl. Opt. 48(9), 1727–1732 (2009).
[16] A. D. Jewell, J. Hennessy, M. E. Hoenk and S. Nikzad, Proc. SPIE 8820, 213–219 (2013).
[17] G. Triani, P. J. Evans, D. R. G. Mitchell, D. J. Attard, K. S. Finnie, et al., Proc. SPIE 5870, 587009 (2005).
[18] R. Ali, M. R. Saleem, P. Pääkkönen and S. Honkanen, Nanomaterials 5(2), 792–803 (2015).
[19] K. Pfeiffer, S. Shestaeva, A. Bingel, P. Munzert, L. Ghazaryan, et al., Opt. Mater. Express 6(2), 660–670 (2016).
[20] Q. Zhang, F. Pan, J. Luo, Q. Wu, Z. Wang, et al., J. Alloys Compd. 659, 288–294 (2016).
[21] Z. Liu, S. Chen, P. Ma, Y. Wei, Y. Zheng, et al., Opt. Express 20(2), 854–863 (2012).
[22] Y. Wei, H. Liu, O. Sheng, Z. Liu, S. Chen, et al., Appl. Opt. 50(24), 4720–4727 (2011).
[23] L. Jensen, J. Maula and D. Ristau, Proc. SPIE 8530, 206–207 (2012).
[24] H. Liu, L. Jensen, J. Becker, M. C. Wurz, P. Ma, et al., Proc. SPIE 10014, 1001421 (2016).
[25] D. Ristau, X. C. Dang and J. Ebert, NBS Spec. Publ. 727, 298–312 (1984).
[26] E. A. Davis and N. F. Mott, Philos. Mag. A 22(179), 903–921 (1970).
[27] ISO 11551, 'Optics and optical instruments – Lasers and laser-related equipment – Test method for absorptance of optical laser components,' (2003).
[28] U. Willamowski, D. Ristau and E. Welsch, Appl. Opt. 37(36), 8362–8370 (1998).
[29] ISO 21254, 'Lasers and laser-related equipment – Test methods for laser-induced damage threshold,' (2011).
[30] M. Mero, J. Liu, W. Rudolph, D. Ristau and K. Starke, Phys. Rev. B 71, 115109 (2005).
[31] C. J. Stolz, M. Caputo, A. J. Griffin and M. D. Thomas, Proc. SPIE 7842, 784206 (2010).
[32] L. Jensen, M. Mende, H. Blaschke, D. Ristau, D. Nguyen, et al., Proc. SPIE 7842, 748207 (2010).